12. Bozano, L., Carter, S., Scott, J., Malliaras, G. & Brock, P. Temperature- and field-dependent electron and hole mobilities in polymer light-emitting diodes. *Appl. Phys. Lett.* **74,** 1132–1134 (1999).
13. Ho, P. K. H. *et al.* Molecular-scale interface engineering for polymer light-emitting diodes. *Nature* **404,** 481–484 (2000).
14. Nagasawa, Y. *et al.* The study of the thermal oxide films on silicon wafers by Fourier transform infrared attenuated total reflection spectroscopy. *J. Appl. Phys.* **68,** 1429–1434 (1990).
15. Dugas, V. & Chevalier, Y. Surface hydroxylation and silane grafting on fumed and thermal silica. *J. Colloid Interf. Sci.* **264,** 354–361 (2003).
16. Perry, C. C. & Li, X. Structural studies of gel phases. *J. Chem. Soc. Faraday Trans.* **87,** 3857–3862 (1991).
17. Tardif, F., Chabli, A., Kanel, A., Rochat, N. & Veillerot, M. Thermal evolution of chemical oxides and (100) silicon at 300 °C in ambient air as seen by attenuated total reflection infrared spectroscopy. *J. Electrochem. Soc.* **150,** G333–G338 (2003).
18. Nicollian, E. H., Berglund, C. N., Schmidt, P. F. & Andrews, J. M. Electrochemical charging of thermal SiO_2 films by injected electron currents. *J. Appl. Phys.* **42,** 5654–5664 (1971).
19. Hartstein, A. & Young, D. R. Identification of electron traps in thermal silicon dioxide films. *Appl. Phys. Lett.* **38,** 631–633 (1981).
20. Malenfant, P. R. L. *et al.* N-type organic thin-film transistor with high field-effect mobility based on a N-N′-dialkyl-3,4,9,10-perylene tetracarboxylic diimide derivative. *Appl. Phys. Lett.* **80,** 2517–2519 (2002).
21. Salleo, A., Chabinyc, M. L., Yang, M. S. & Street, R. A. Polymer thin-film transistors with chemically modified dielectric interfaces. *Appl. Phys. Lett.* **81,** 4383–4385 (2002).
22. Angst, D. L. & Simmons, G. W. Moisture absorption characteristics of organosiloxane self-assembled monolayers. *Langmuir* **7,** 2236–2242 (1991).
23. Wasserman, S. R., Tao, Y. T. & Whitesides, G. M. Structure and reactivity of alkylsiloxane monolayers formed by reaction of alkyltrichlorosilanes on silicon substrates. *Langmuir* **5,** 1074–1087 (1989).
24. Sirringhaus, H. *et al.* Two-dimensional charge transport in self-organised, high-mobility conjugated polymers. *Nature* **401,** 685–688 (1999).
25. Wilson, R. J. *Polymer Field-effect Transistors from Polyfluorene-based Conjugated Polymers.* PhD thesis, Univ. Cambridge (2002).

Supplementary Information accompanies the paper on **www.nature.com/nature**.

Acknowledgements We thank A. Achen for providing the BCB material, which is commercially available as Dow Cyclotene, and Merck KGaA for P3HT. L-L.C. and J-F.C. thank the EPSRC Carbon-Based Electronics programme for support, and J.Z. thanks the Gates Cambridge Trust for support. P.K-H.H. thanks St John's College for a research fellowship, the National University of Singapore for research support, and S. J. Chua for technical discussions, support and access to laboratory facilities. We also thank C.-C. Chum for technical support.

Competing interests statement The authors declare competing financial interests: details accompany the paper on **www.nature.com**.

Correspondence and requests for materials should be addressed to P.K.-H.H. (phyhop@nus.edu.sg) and R.H.F. (rhf10@cam.ac.uk).

Ultrafast memory loss and energy redistribution in the hydrogen bond network of liquid H_2O

M. L. Cowan[1]*, B. D. Bruner[1]*, N. Huse[2]*, J. R. Dwyer[1], B. Chugh[1], E. T. J. Nibbering[2], T. Elsaesser[2] & R. J. D. Miller[1]

[1]*Departments of Chemistry and Physics, University of Toronto, 80 St George Street, Toronto, Ontario, Canada M5S3H6*
[2]*Max-Born-Institut für Nichtlineare Optik und Kurzzeitspektroskopie, Max-Born-Strasse 2A, D-12489 Berlin, Germany*

* These authors contributed equally to this work

Many of the unusual properties of liquid water are attributed to its unique structure, comprised of a random and fluctuating three-dimensional network of hydrogen bonds that link the highly polar water molecules[1,2]. One of the most direct probes of the dynamics of this network is the infrared spectrum of the OH stretching vibration[3–11], which reflects the distribution of hydrogen-bonded structures and the intermolecular forces controlling the structural dynamics of the liquid. Indeed, water dynamics has been studied in detail[5–14], most recently using multi-dimensional nonlinear infrared spectroscopy[15,16] for acquiring structural and dynamical information on femtosecond timescales. But owing to technical difficulties, only OH stretching vibrations in D_2O or OD vibrations in H_2O could be monitored. Here we show that using a specially designed, ultrathin sample cell allows us to observe OH stretching vibrations in H_2O. Under these fully resonant conditions, we observe hydrogen bond network dynamics more than one order of magnitude faster than seen in earlier studies that include an extremely fast sweep in the OH frequencies on a 50-fs timescale and an equally fast disappearance of the initial inhomogeneous distribution of sites. Our results highlight the efficiency of energy redistribution within the hydrogen-bonded network, and that liquid water essentially loses the memory of persistent correlations in its structure within 50 fs.

The high optical density of the OH stretching mode in pure H_2O and parasitic window signals in conventional samples have so far

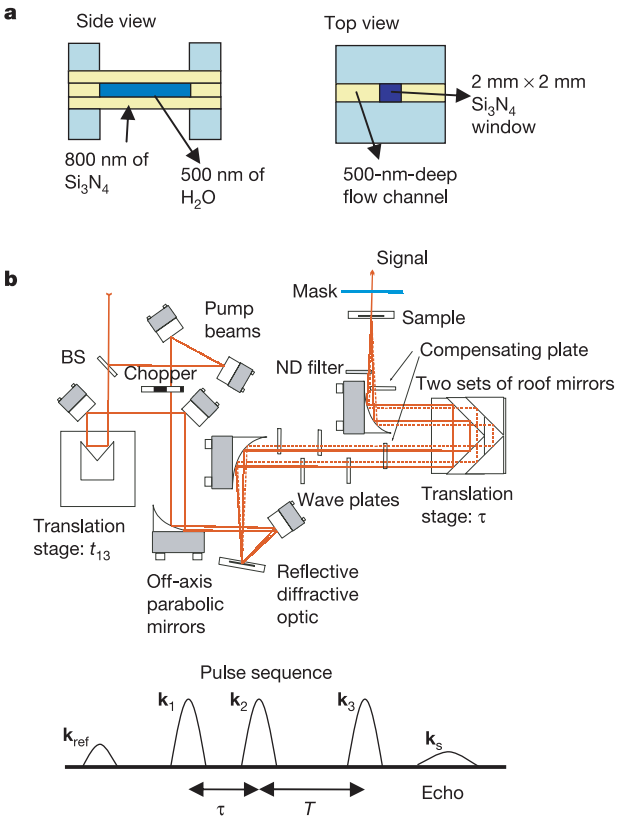

Figure 1 Experimental set-up. **a**, Nanofluidic sample cell: Each Si_3N_4 window has a 2 mm × 2 mm clear aperture and is 800 nm thick, which provides the necessary structural support for a stable sample, yet is thin enough to give a negligible non-resonant window signal. The windows were also coated with a 10-nm SiO_2 layer to ensure that their surfaces are sufficiently hydrophilic to allow effective capillary flow of the water into the cell and uniform distribution of the water once inside. **b**, Schematic of two-dimensional infrared experiment: The 70-fs pulse from a mid-IR Optical Parametric Amplifier is split into two at a beam splitter (BS), and one is given a variable delay t_{13} using a retroreflector on a translation stage. The two beams are focused onto a reflective diffractive optic at a small angle to each other, using an off-axis parabolic mirror. The diffractive optic is optimized to diffract 70% of the intensity of each beam into the ±1 diffraction orders. The resulting four beams lie at the corners of a square, forming a 'boxcar' pattern. Using the second translation stage, the bottom two beams are then delayed by a time τ. This results in the pulse sequence shown, with the two pump beams ($\mathbf{k}_1$, $\mathbf{k}_2$) separated by the coherence time τ and the second pump and probe beam ($\mathbf{k}_2$, $\mathbf{k}_3$) separated by the population time T. The fourth beam in the boxcar pattern is the weak reference pulse $\mathbf{k}_{ref}$, which is attenuated by the neutral density (ND) filter and passed through the sample cell before the excitation pulses ($\mathbf{k}_1$, $\mathbf{k}_2$, $\mathbf{k}_3$). The 1-μJ pulses are then focused to a 150-μm spot in the sample, and the signal is heterodyne detected, using the fourth beam as a local oscillator. Under these conditions, the temperature rise in the sample measured using a thermal imaging camera was less than 8 K above room temperature.

hindered attempts to access the fastest relaxation processes of liquid water in pure H_2O. To overcome these problems, we designed the nanofluidic cell illustrated in Fig. 1a—extremely thin (800 nm) Si_3N_4 windows remove nonlinear window signals, while the similarly thin (500 nm) water layer has a peak optical density of only 0.2. The experiment uses our spectroscopy method based on diffractive optics[17] and involves applying three ~1-μJ, 70-fs pulses centred at 3,350 cm^{-1} in the OH stretching band to generate photon echoes as a function of the coherence time τ and the population time T, as shown in Fig. 1b. The photon echo signal is heterodyne-detected by spectral interferometry[17–19] with a reference pulse from the same mid-infrared source, directly giving the echo as a function of the detected frequency dimension ν_3. The coherence time τ is then scanned at constant population time T and the signal is Fourier-transformed along the τ dimension to produce the excitation frequency dimension ν_1. The absorptive part of the resulting two-dimensional infrared spectrum is determined by fitting phase factors to independently measured spectrally resolved pump–probe data[12,17,19].

Figure 2 shows spectrally integrated transient grating measurements for population times T up to 2 ps for both parallel and perpendicular polarizations. Both polarization conditions exhibit a fast exponential decay with a 95-fs time constant, followed by a rise with a 1.3-ps time constant at later times T. On this timescale, energy transfer processes can influence the polarization anisotropy[6] (Fig. 2), that is, energy transfer from the preferentially excited OH vibrations along the excitation polarization direction to different water molecules leads to a decay in the degree of polarization of the signal. The polarization anisotropy decays exponentially with a 75-fs time constant, substantially shorter than the 700-fs time constant we measure in a diluted 6:1 D_2O:H_2O mixture under the same conditions in our nanofluidic cell (see Supplementary Information); this 700-fs time constant is in agreement with pump–probe measurements previously taken with 200-fs pulses[6].

By heterodyne detecting and spectrally resolving the transient grating signal, we gain much more detailed information about the dynamics of the system. Figure 3 shows the absorptive part of the spectrally resolved transient grating signal with the polarization of all three pulses parallel. At $T = 0$, the positive peak corresponds to reduced absorption (bleaching) caused by the depletion of the $\nu = 0$ state of the OH stretching oscillator and stimulated emission from the $\nu = 1$ state. The negative peak corresponds to excited state absorption of the $\nu = 1$ to $\nu = 2$ transition, which is red-shifted from the $\nu = 0$ to $\nu = 1$ transition, owing to the strong anharmonicity of the OH stretching oscillator. The time evolution of such signals depends strongly on the spectral position. The enhanced absorption below 3,000 cm^{-1} and the bleaching above 3,500 cm^{-1} display a very fast decay that is close to the 50-fs time resolution of our experiment. A substantially slower decay and a subsequent picosecond timescale rise are observed between 3,170 and 3,400 cm^{-1}, at the centre of the bleaching contribution. Such comparably slow components dominate the spectrally integrated kinetics shown in Fig. 2.

Two-dimensional infrared spectra at different population times are shown in Fig. 4. The absorptive component of the echo signal is plotted. At $T = 0$, such spectra display an on-diagonal peak due to bleaching and stimulated emission of the $\nu = 0$ to $\nu = 1$ transition and an off-diagonal absorption peak due to the $\nu = 1$ to 2 transition. At $T = 0$, the on-diagonal peak is stretched along the diagonal, indicating inhomogeneous broadening. At $T = 50$ fs, this inhomogeneity is almost entirely lost (>90% based on curvature of the line contours), and by $T = 100$ fs it is completely gone. The excited-state peak off the diagonal in Fig. 4 decays on the same timescale, in agreement with the transient grating results of Fig. 3. Most importantly, there are extremely fast processes that wash out the structural variations (inhomogeneous broadening), such that the OH stretching excitation loses its memory on extraordinarily fast timescales, faster than in any other liquid.

Liquid water represents a disordered ensemble of highly polar molecules linked through a fluctuating network of intermolecular hydrogen bonds. The transition frequency of an individual OH stretching oscillator in this system depends on the local environment, resulting in an inhomogeneous broadening of the OH stretching band of the order of several hundreds of cm^{-1}. In addition, the OH stretching oscillators on different water molecules are coupled through hydrogen bonds and through other mechanisms, for example, dipole–dipole coupling, that lead to rapid

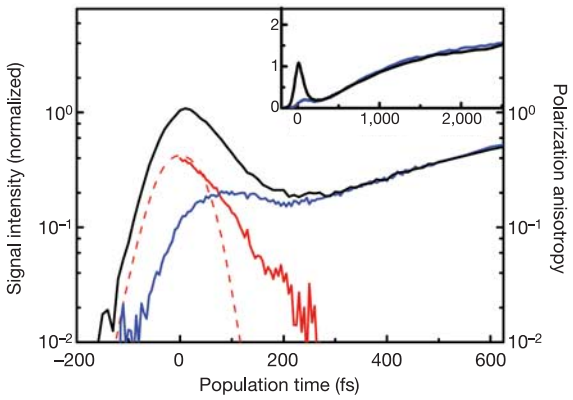

Figure 2 Spectrally integrated transient grating data in pure H_2O. The parallel polarization [0°, 0°, 0°, 0°] (black line) and crossed probe polarization [0°, 0°, 90°, 90°] (blue line) data show a fast initial decay of the population, followed by a thermal grating rise due to vibrational relaxation on a picosecond timescale. The dashed red line shows the pulse-width limited response that is convolved with a bi-exponential to determine the decay rates. The polarization anisotropy (red line), shows the fast sub-100 fs energy transfer of pure H_2O. Inset, longer time dynamics. The initial value of the polarization anisotropy is 0.4, as expected for the excitation of individual linear transition dipole moments.

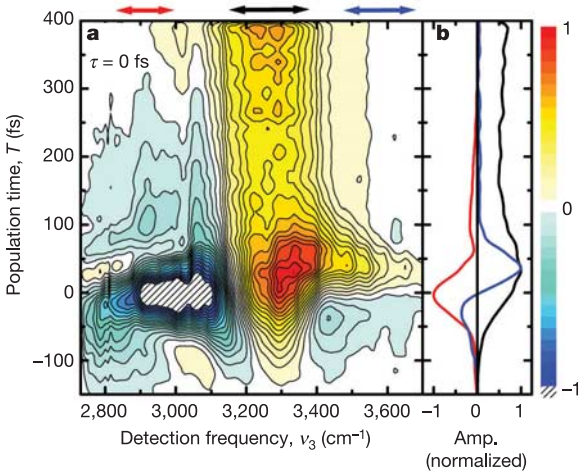

Figure 3 Absorptive component of the spectrally resolved transient grating signal, plotted as a function of population time T. **a**, This shows the fast spectral diffusion and excited state decay, and the beginning of the thermal grating rise due to vibrational relaxation. **b**, Normalized amplitude (Amp.) of the transient grating signal spectrally integrated in three windows, on the red (red line), middle (black line) and blue (blue line) sides of the spectrum. The data are not corrected for the slight frequency chirp of the femtosecond pulses. Independent pulse characterization by frequency-resolved optical gating shows that the signals rise within the time resolution of the experiment at all detection frequencies, that is, also for detection frequencies above 3,400 cm^{-1}. Spectral diffusion dominates the fast decay of the red and blue regions, while population dynamics dominate the centre of the spectrum. The contour scale is displayed from −1 to 1 in order to focus on the region of interest.

transfer of vibrational energy between neighbouring molecules. Gas-phase studies of water clusters and theoretical calculations have shown that the coupling between OH oscillators is small compared to the disorder-related inhomogeneous broadening[20,21]. Taking this and the very short excitation pulses into consideration, we can think of the OH excitation as initially localized on a particular microscopic configuration of water molecules that then evolves over time. Nuclear motions, excitation transfer and couplings due to the highly polar nature of water open up relaxation channels and configuration-averaging mechanisms that are absent in other liquids.

The spectrally resolved transient-grating data (Fig. 3) display a very fast component on the red and blue edges, and in addition, slower kinetics in the centre of the OH stretching band. The slow component observed between 3,170 and 3,400 cm^{-1} reflect the population kinetics of the excited OH stretching oscillators. The $\tau_1 = 95$ fs decay of the transient grating signal corresponds to a depopulation of the $\nu = 1$ state with $T_1 = 2\tau_1 = 190$ fs, with possible short-lived intermediates contributing through terms connected to the ground-state recovery. The slower 1.3-ps rise of the spectrally integrated transient-grating signal at late population times (inset of Fig. 2) is attributed to heating effects associated with vibrational relaxation, similar to the behaviour found in spectrally resolved infrared pump–probe and infrared pump–Raman-probe studies of water[22,23]. The 75-fs decay in the polarization anisotropy (Fig. 2) is attributed to energy transfer among the OH stretching vibrations. We note that depolarization of the OH excitation requires the excitation sampling of several different waters within the pentameric structure of hydrogen-bonded water molecules and we can infer that this timescale is an upper limit for the excitation hopping time.

We observe an extremely fast sub-100-fs component of spectral diffusion below 3,000 cm^{-1} and above 3,500 cm^{-1}. Our results point to a blueshift of the $\nu = 1$ to $\nu = 2$ transition and a simultaneous red-shift of the $\nu = 0$ to $\nu = 1$ transition on a 50-fs timescale. This finding suggests ultrafast structural changes by which the dipole induced on the $\nu = 0$ to $\nu = 1$ transition is solvated[24], thus lowering the energy of the $\nu = 1$ state of the oscillator. This solvation process is distinct from solvent repolarization involved in electronic transitions because the induced dipole changes with OH excitation are much smaller in magnitude and there are also local interactions through hydrogen bonding. Rather, this effect is related to fluctuations local to the excited OH that change the effective degree of hydrogen bonding. The timescale of the fastest spectral diffusion processes is definitely shorter than the 200-fs period of the O–H..O hydrogen-bond mode (frequency 170 cm^{-1}) and other reorientation and energy transfer processes occurring in the subpicosecond to picosecond time domain.

We conclude that structural dynamics related to such degrees of freedom plays a minor part in the ultrafast loss of memory observed here. Instead, we consider fast librational motions (hindered rotations), which are the relevant excitations in the hydrogen-bonded network[25–27]. The low-frequency vibrational spectrum of liquid H_2O displays a pronounced band between 300 and 1,000 cm^{-1} that originates from librational excitations with periods between 90 and 30 fs, the latter being in the relevant time range to account for the speed of both the spectral diffusion in Fig. 3 and the dephasing in Fig. 4. Energy transfer processes on a somewhat slower timescale also contribute to the observed spectral diffusion and loss of memory, although they do not dominate the process—as might be expected from extrapolations of other isotopic studies of liquid water[6,28].

We have studied pure H_2O to determine the microscopic processes leading to energy redistribution in the fully resonant hydrogen-bond network. This work demonstrates the loss of memory of persistent correlations in water structure within 50 fs that favours rapid relaxation of elementary excitations and is probably important in stabilizing biological systems coupled to this network of hydrogen bonds. □

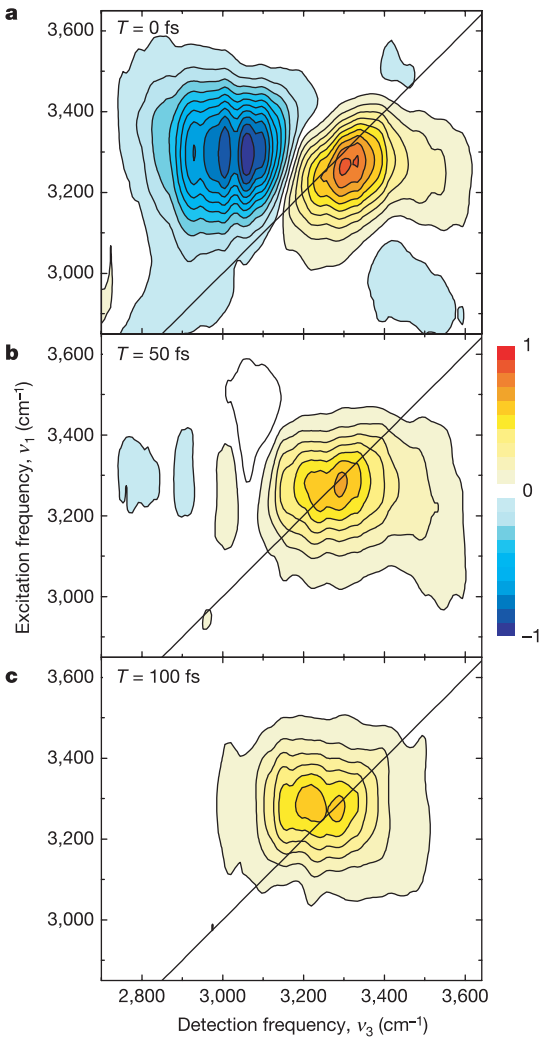

Figure 4 Absorptive components of the two-dimensional-infrared echo spectra of pure liquid H_2O for different population times. **a**, $T = 0$ fs; **b**, $T = 50$ fs; **c**, $T = 100$ fs. The inhomogeneity indicated by the stretching of the positive peak along the diagonal in the $T = 0$ spectrum has almost completely decayed by $T = 50$ fs, clearly showing the very rapid dephasing and loss of memory in the system.

Received 18 October 2004; accepted 21 January 2005; doi:10.1038/nature03383.

1. Eisenberg, D. & Kauzmann, W. *The Structure and Properties of Water* (Oxford Univ. Press, New York, 1969).
2. Franks, F. (ed.) *Water, a Comprehensive Treatise* (Plenum, New York, 1972).
3. Luzar, A. & Chandler, D. Hydrogen-bond kinetics in liquid water. *Nature* **379,** 55–57 (1996).
4. Marx, D., Tuckerman, M. E., Hutter, J. & Parrinello, M. The nature of the hydrated excess proton in water. *Nature* **397,** 601–604 (1999).
5. Graener, H., Seifert, G. & Laubereau, A. New spectroscopy of water using tunable picosecond pulses in the infrared. *Phys. Rev. Lett.* **66,** 2092–2095 (1991).
6. Woutersen, S. & Bakker, H. J. Resonant intermolecular transfer of vibrational energy in liquid water. *Nature* **402,** 507–509 (1999).
7. Gale, G. M. *et al.* Femtosecond dynamics of hydrogen bonds in liquid water: A real-time study. *Phys. Rev. Lett.* **82,** 1068–1071 (1999).
8. Stenger, J., Madsen, D., Hamm, P., Nibbering, E. T. J. & Elsaesser, T. Ultrafast vibrational dephasing of liquid water. *Phys. Rev. Lett.* **87,** 027401 (2001).
9. Møller, K. B., Rey, R. & Hynes, J. T. Hydrogen bond dynamics in water and ultrafast infrared spectroscopy: a theoretical study. *J. Phys. Chem. A* **108,** 1275–1289 (2004).
10. Lawrence, C. P. & Skinner, J. L. Vibrational spectroscopy of HOD in liquid D_2O. Infrared line shapes and vibrational Stokes shift. *J. Chem. Phys.* **117,** 8847–8854 (2002).
11. Torre, R., Bartolini, P. & Righini, R. Structural relaxation in supercooled water by time-resolved spectroscopy. *Nature* **428,** 296–299 (2004).

12. Asbury, J. B. *et al.* Water dynamics: vibrational echo correlation spectroscopy and comparison to molecular dynamics simulations. *J. Phys. Chem. A* **108,** 1107–1119 (2004).
13. Fecko, C. J., Eaves, J. D., Loparo, J. J., Tokmakoff, A. & Geissler, P. L. Ultrafast hydrogen-bond dynamics in the infrared spectroscopy of water. *Science* **301,** 1698–1702 (2003).
14. Stenger, J., Madsen, D., Hamm, P., Nibbering, E. T. J. & Elsaesser, T. A photon echo peak shift study of liquid water. *J. Phys. Chem. A* **106,** 2341–2350 (2002).
15. Asplund, M. C., Zanni, M. T. & Hochstrasser, R. M. Two dimensional infrared spectroscopy of peptides by phase-controlled femtosecond vibrational photon echoes. *Proc. Natl Acad. Sci. USA* **97,** 8219–8224 (2000).
16. Mukamel, S. Multidimensional femtosecond correlation spectroscopies of electronic and vibrational excitations. *Annu. Rev. Phys. Chem.* **51,** 691–729 (2000).
17. Cowan, M. L., Ogilvie, J. P. & Miller, R. J. D. Two-dimensional spectroscopy using diffractive optics based phased-locked photon echoes. *Chem. Phys. Lett.* **386,** 184–189 (2004).
18. Lepetit, L., Cheriaux, G. & Joffre, M. Linear techniques of phase measurement by femtosecond spectral interferometry for applications in spectroscopy. *J. Opt. Soc. Am. B* **104,** 2467–2474 (1995).
19. Hybl, J. D., Albrecht, A. W., Faeder, S. M. G. & Jonas, D. M. Two-dimensional electronic spectroscopy. *Chem. Phys. Lett.* **297,** 307–313 (1998).
20. Rice, S. A., Bergren, M. S., Beich, A. C. & Nielson, G. A theoretical analysis of the OH stretching spectra of ice Ih, liquid water, and amorphous solid water. *J. Phys. Chem.* **87,** 4295–4308 (1983).
21. Wojcik, M. J., Buch, V. & Devlin, J. P. Spectra of isotopic ice mixtures. *J. Chem. Phys.* **99,** 2332–2344 (1993).
22. Lock, A. J. & Bakker, H. J. Temperature dependence of vibrational relaxation in liquid H_2O. *J. Chem. Phys.* **117,** 1708–1713 (2002).
23. Pakoulev, A., Wang, Z. & Dlott, D. Vibrational relaxation and spectral evolution following ultrafast OH stretch excitation of water. *Chem. Phys. Lett.* **371,** 594–600 (2003).
24. Jimenez, R., Fleming, G. R., Kumar, P. V. & Maroncelli, M. Femtosecond solvation dynamics in water. *Nature* **369,** 471–473 (1994).
25. Castner, E. W. Jr, Chang, Y. J., Chu, Y. C. & Walrafen, G. E. The intermolecular dynamics of liquid water. *J. Chem. Phys.* **102,** 653–659 (1995).
26. Saito, S. & Ohmine, I. Third order nonlinear response of liquid water. *J. Chem. Phys.* **106,** 4889–4893 (1997).
27. Pohorille, A., Pratt, L. R., LaViolette, R. A., Wilson, M. A. & MacElroy, R. D. Comparison of the structure of harmonic aequous glasses and liquid water. *J. Chem. Phys.* **87,** 6070–6077 (1987).
28. Poulsen, J. A., Nyman, G. & Nordholm, S. Wave packet study of ultrafast relaxation in ice Ih and liquid water. Resonant intermolecular vibrational energy transfer. *J. Phys. Chem. A* **107,** 8420–8428 (2003).

Supplementary Information accompanies the paper on **www.nature.com/nature**.

Acknowledgements We thank F. Weik for help with the use of a thermal imaging camera. Financial support by the Deutsche Forschungsgemeinschaft, the Humboldt foundation (R.J.D.M.), the Canadian Foundation for Innovation, the Natural Sciences and Engineering Research Council of Canada, and Photonics Research Ontario is acknowledged.

Competing interests statement The authors declare that they have no competing financial interests.

Correspondence and requests for materials should be addressed to R.J.D.M. (rjdmiller@lphys.chem.utoronto.ca).

The formation of cubic ice under conditions relevant to Earth's atmosphere

Benjamin J. Murray, Daniel A. Knopf & Allan K. Bertram

Department of Chemistry, University of British Columbia, 2036 Main Mall, Vancouver, British Columbia V6T 1Z1, Canada

An important mechanism for ice cloud formation in the Earth's atmosphere is homogeneous nucleation of ice in aqueous droplets, and this process is generally assumed to produce hexagonal ice[1,2]. However, there are some reports that the metastable crystalline phase of ice, cubic ice, may form in the Earth's atmosphere[3–5]. Here we present laboratory experiments demonstrating that cubic ice forms when micrometre-sized droplets of pure water and aqueous solutions freeze homogeneously at cooling rates approaching those found in the atmosphere. We find that the formation of cubic ice is dominant when droplets freeze at temperatures below 190 K, which is in the temperature range relevant for polar stratospheric clouds and clouds in the tropical tropopause region. These results, together with heat transfer calculations, suggest that cubic ice will form in the Earth's atmosphere. If there were a significant fraction of cubic ice in some cold clouds this could increase their water vapour pressure, and modify their microphysics and ice particle size distributions[5]. Under specific conditions this may lead to enhanced dehydration of the tropopause region[5].

An important mechanism for ice cloud formation in the Earth's atmosphere is homogeneous nucleation of ice in aqueous droplets. For example, polar stratospheric clouds, which play a key role in stratospheric ozone depletion, can form by homogeneous freezing of HNO_3-H_2SO_4-H_2O droplets at temperatures below 189 K (ref. 6). Also, ice cirrus clouds, which play an important role in the Earth's climate[7], can form through the homogeneous freezing of NH_3-H_2SO_4-H_2O droplets at temperatures below 235 K (ref. 8). Nevertheless, the crystalline phase of ice that forms when aqueous droplets freeze in the atmosphere is unknown. Before this study, cubic ice (ice I_c) has been made in the laboratory using extremely fast cooling rates[9–13], by annealing the amorphous phase[14,15], and by freezing of water in nano-porous silica[16]. The conditions used to produce ice I_c in these previous studies are significantly different from the conditions at which ice clouds form in the Earth's atmosphere. The crystalline form of ice that precipitates in water has also been investigated theoretically. For example, thermodynamic considerations suggest that the free energy involved in forming an ice I_c nucleus are more favourable than those needed to form a nucleus of hexagonal ice (ice I_h)[17,18]. In addition, molecular-dynamics simulations found that ice I_c crystallizes in electric fields[19] and a variant of ice IX forms when the water density is 1.15 and 1.20 g cm^{-3} (ref. 20). However, the crystal structure that forms under typical atmospheric conditions is unclear from theoretical studies. In the present experimental study we investigate the phase of ice that forms when pure water and aqueous solution droplets (solute = $(NH_4)_3H(SO_4)_2$, HNO_3, $(NH_4)_2SO_4$ or NaCl) freeze homogeneously, while being cooled at rates approaching those found in the atmosphere.

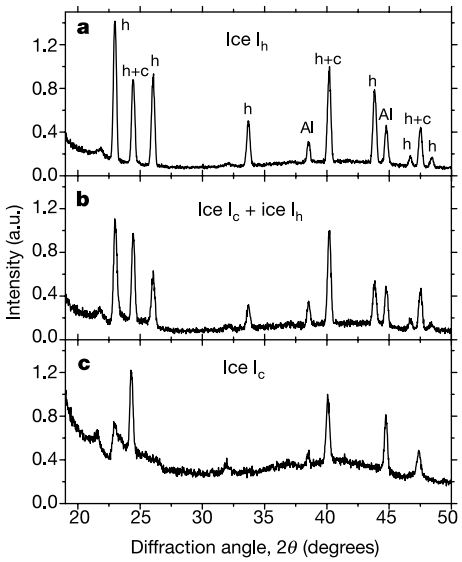

Figure 1 X-ray diffraction patterns of frozen aqueous droplets. The droplets homogeneously froze as the temperature of the cell was decreased at a rate of 10 K min^{-1}. **a**, Diffraction pattern of pure water, which froze at 235 ± 2 K and was annealed at 268 K for 35 min. **b**, Pattern for the same sample of pure water as in **a** before it was annealed. **c**, Diffraction pattern of 43 wt% $(NH_4)_3H(SO_4)_2$ solution droplets that froze at 188 ± 2 K. Reflections unique to ice I_h are labelled h and those common to both ice I_c and I_h are labelled h+c. Each of the diffraction patterns has been normalized to the peak at 40°. Minor peaks at 22° and 32° are reflections from the Teflon and grease. Major peaks marked 'Al' are reflections from the aluminium cooling cell.